Enhancing Luminescence in Lanthanide-Doped Upconversion Nanoparticles

Sanyang Han, Renren Deng, Xiaoji Xie, and Xiaogang Liu*

The enthusiasm for research on lanthanide-doped upconversion nanoparticles is driven by both a fundamental interest in the optical properties of lanthanides embedded in different host lattices and their promise for broad applications ranging from biological imaging to photodynamic therapy. Despite the considerable progress made in the past decade, the field of upconversion nanoparticles has been hindered by significant experimental challenges associated with low upconversion conversion efficiencies. Recent experimental and theoretical studies on upconversion nanoparticles have, however, led to the development of several effective approaches to enhancing upconversion luminescence, which could have profound implications for a range of applications. Herein we present the underlying principles of controlling energy transfer through lanthanide doping, overview the major advances and key challenging issues in improving upconversion luminescence, and consider the likely directions of future research in the field.

1. Introduction

Lanthanide-doped upconversion nanoparticles (UCNPs) have the remarkable ability to combine two or more low-energy photons to generate a single high-energy photon by an anti-Stokes process and hold great promise for a broad range of applications, ranging from high-resolution bioimaging to modern photovoltaic technologies.[1] In contrast to conventional luminescent probes, lanthanide-doped UCNPs exhibit excellent photostability, continuous emission capability, and sharp multi-peak line emission. Furthermore, with near-infrared (NIR) excitation, light scattering by biological tissues is substantially reduced. The reduction in light scattering by NIR excitation results in a depth of penetration in tissue much larger than that obtained under ultraviolet or visible excitation.[2] Notably, the excitation of these nanoparticles with a NIR light source eliminates background interference from either endogenous fluorophores or non-specifically bound probes, thus enabling quantitative analysis of molecular interaction in biological samples.[3] The UCNPs also have luminescence decay times on the order of microseconds, which are much longer than those of organic dyes and quantum dots (typically 0.1–20 ns). With a time-gated intensity detector, the short-lived autofluorescence emitted by biological specimens on excitation can be completely separated from the long-lived luminescence from the UCNPs.[4]

It is important to note that the use of UCNPs also permits the minimization of non-absorption energy losses in photovoltaic devices by transforming sub-bandgap NIR photons into usable above-bandgap photons. This development provides an exciting opportunity to surpass the Shockley–Queisser efficiency limit.[5] However, UCNPs often suffer from low quantum efficiencies and strong luminescence quenching in aqueous solvents, largely because of the comparatively low extinction coefficients of lanthanide dopants. Innovative ways have been developed to synthesize high quality, biocompatible UCNPs displaying much improved optical properties. Despite significant progress, the control and manipulation of the energy transfer on the nanoscale by lanthanide doping are less well understood. In this Minireview, we attempt to provide a concise survey of several approaches that can be used to enhance upconversion luminescence in lanthanide-doped nanocrystals (Figure 1). These include host lattice manipulation, energy transfer

[*] S. Han, Dr. R. Deng, Dr. X. Xie, Prof. X. Liu
Department of Chemistry, National University of Singapore
Science Drive 3, Singapore 117543 (Singapore)
E-mail: chmlx@nus.edu.sg

Prof. X. Liu
Institute of Materials Research and Engineering
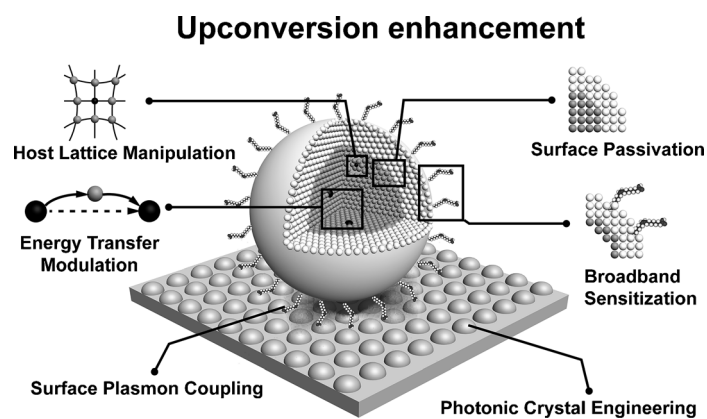Research Link, Singapore 117602 (Singapore)

Upconversion enhancement

Figure 1. Schematic illustration of the main strategies for enhancing luminescence in lanthanide-doped UCNPs. Note that the enhancement in the upconversion luminescence in many cases is achieved through synergistic effects by combining several strategies.

modulation, surface passivation, surface plasmon coupling, broadband sensitization, and photonic crystal engineering.

2. Strategies for Enhancing Upconversion Luminescence

2.1. Host Lattice Manipulation

The lanthanides, typically existing in their most stable oxidation state as trivalent ions (Ln^{3+}), are extensively studied for their optical properties. The lanthanide ions feature an electron configuration of $4f^n$ ($0 < n < 14$) and the

arrangements of electrons within this configuration are substantially diverse (Figure 2a). The energy levels of free Ln^{3+} ions in 4f orbitals are determined by, in order of importance, the Coulombic interaction and the spin-orbit coupling between f electrons. The Coulombic interaction, which represents the mutual repulsion of the electrons, generates the total orbital angular momentum (L) and total spin angular momentum (S). Furthermore, the spin-orbit coupling makes the total angular momentum (J) of the f-electrons. Each set of L, S, and J corresponds to a specific distribution of electrons within the 4f-shell and defines a particular energy level. We can derive the energy level of the free ions using the term symbols of $^{2S+1}L_J$ according to the
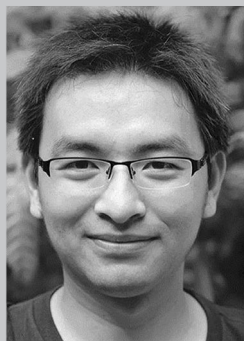
Sanyang Han was born in Hubei, China. He received his BS (2007) and MS (2010) degrees in Chemistry from Soochow University. He is currently pursuing a Ph.D. degree under the supervision of Professor Xiaogang Liu at the National University of Singapore. His research interests focuses on the development of novel lanthanide-doped luminescent nanomaterials for bioimaging and therapeutic applications.

Xiaoji Xie was born in Jiangsu, China. He earned his BS (2009) degree in chemistry from Nanjing University. He completed his Ph.D. (2014) at the National University of Singapore with Professor Xiaogang Liu, where he worked on the development and applications of metal nanoparticles for biological sensing. He is currently a postdoctoral researcher working in collaboration with Professor Xiaogang Liu. His current research involves the investigation of upconversion nanoparticles that can be effectively excited with tunable wavelengths.
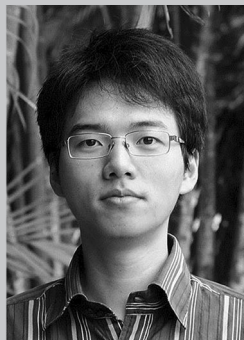
Renren Deng was born in Sichuan, China. He earned his BS degree in 2009 from Zhejiang University. He then completed his Ph.D. on enhancing multiphoton upconversion at the National University of Singapore in 2014 under the direction of Professor Xiaogang Liu. He is currently working as a postdoctoral researcher in the same group. His research interests are in developing novel materials for volumetric 3D display and understanding energy transfer through lanthanide-doped nanoparticles.
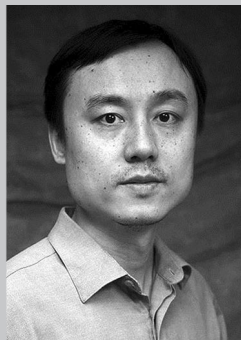
Xiaogang Liu was born and raised in Jiangxi, China. He received his Ph.D. from Northwestern University in 2004 with professor Chad Mirkin before his postdoctoral studies with Professor Francesco Stellacci at MIT. In 2006, he joined the faculty of the National University of Singapore as an assistant professor. In 2011, he took a joint appointment with the Institute of Materials Research and Engineering, Agency for Science, Technology and Research (A*STAR). His interests include lanthanide-doped optical nanomaterials, supramolecular chemistry, and surface science for catalysis, sensors and biomedical applications.
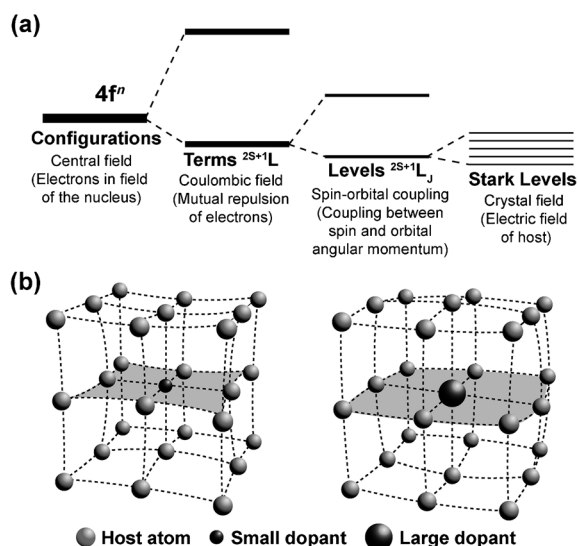
Figure 2. a) Simplified representation of the effect of Coulombic field, spin-orbit coupling, and crystal-field interaction on the [Xe]4f^n configuration. b) Crystal lattice contraction (left) and expansion (right) as a result of the substitution of a host atom with a dopant of varied size.

Russell–Saunders notation, where $2S + 1$ represents the total spin multiplicity.[6]

Lanthanide luminescence mainly originates from the electron transition within the 4f^n configuration that consists of enormously complex energy levels owing to the spin-orbit coupling and crystal field interaction. In principle, the f–f transitions are parity-forbidden. However, mixing of opposite-parity configurations can lead to the breakdown of the selection rule where electric dipole transitions are weakly allowed. In response to an asymmetric crystal field, the probability of the electric dipole transitions is greatly increased. Therefore, lowering the symmetry around the lanthanides by tailoring the crystal structure may enhance luminescence emission intensity.

The crystal lattices of lanthanide-doped nanocrystals can be modified by ion doping for enhanced upconversion luminescence as different sized ions could dramatically influence the coordination environment and crystal field splitting of lanthanides (Figure 2b).[7] The lithium ion is the smallest metallic ion in the periodic table with an ionic radius of 0.9 Å. As such, Li$^+$ ions can be easily incorporated into the host lattices. Early examples of lithium doping were demonstrated in oxide host lattices. For example, Chen et al. reported 25- and 60-fold enhancements in the respective green and violet emission of Y_2O_3:Yb/Er nanophosphors through lithium doping.[8] The versatility of the lithium-doping approach for enhanced upconversion luminescence was later validated by a number of research groups in other oxide host matrices, including TiO_2,[9] $BaTiO_3$,[10] ZrO_2,[11] ZnO,[12] $ZnWO_4$,[13] $Y_3Al_5O_{12}$,[14] $CaMoO_4$,[15] and $GdVO_4$.[16]

Alternatively, Li$^+$ ions can be inserted into fluoride host lattices for increased upconversion luminescence. In comparison with oxides, fluorides usually exhibit low phonon energies and high chemical stability. In 2009, Nann and Wang reported a 30-fold increase in emission intensity of Er^{3+} using

Li$^+$-doped $NaYF_4$ host materials.[17] As a separate study, Zhang and co-workers observed an eightfold enhancement of Tm^{3+} emission in Li$^+$-doped $NaYF_4$ nanoparticles.[18] In addition, gadolinium-based materials have also been examined for luminescence enhancement through lithium doping.[19] The Li$^+$ ions were incorporated into the GdF_3 (or $NaGdF_4$) nanoparticles by mixing Li$^+$ ions with the gadolinium precursors formulated to make the nanophosphors. The combination of upconverted emission with intriguing magnetic properties makes these nanoparticles particularly useful as dual-modal probes for biomedical applications.

Doping of transition-metal ions together with lanthanides in nanocrystals can also lead to enhanced upconversion luminescence. This enhancement is attributed to the strengthening of the electron–phonon coupling and much improved susceptibility to crystal-field and exchange perturbations, because the d orbitals of transition metals have larger radial extension than the f orbitals of lanthanides. Successful examples of enhancing upconversion emission through transition-metal doping include Zn^{2+}, Bi^{3+}, Fe^{3+}, and Sc^{3+} in oxide and fluoride host lattices with lanthanide activators.[20] For better understanding of upconversion dynamics, a major issue that needs to be addressed is the statistical distribution of dopant ions within an individual nanocrystal.

Compared to the conventional chemical doping approaches, the variation of crystal lattices by a physical method is desirable as it allows for in situ and real-time modulation of upconversion emission. Recently, Hao et al.[21] developed an electric-field-induced enhancement of upconversion luminescence. In their study, a ferroelectric host material ($BaTiO_3$) was chosen and doped with Yb^{3+} and Er^{3+} to produce a $BaTiO_3$:Yb/Er film. They then varied the structural symmetry of the $BaTiO_3$ host by applying a direct current bias voltage (Figure 3a). A 2.7-fold enhancement of green
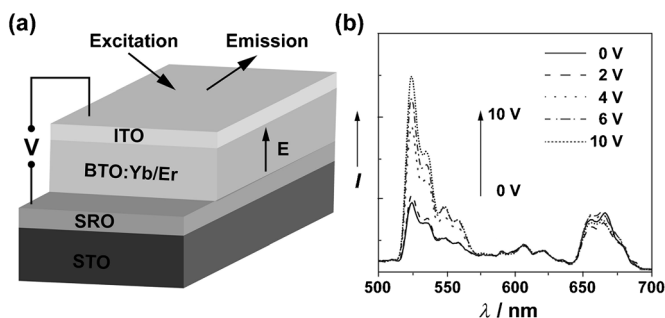

Figure 3. a) The setup used to measure the upconversion emission of BTO:Yb/Er thin film by applying an external electric field. ITO = indium tin oxide, BTO = $BaTiO_3$, SRO = $SrRuO_3$, and STO = $SrTiO_3$. b) The upconversion emission spectra of the BTO:Yb/Er film under a direct current bias voltage ranging from 0 to 10 V. Adapted with permission from Ref. [21].

upconversion emission was observed when the bias voltage was increased to 10 V (Figure 3b). However, the red emission of the film was not enhanced by changing the bias voltage, suggesting the wavelength-dependent nature of the emission enhancement. The enhancement and modulation of upconversion luminescence under the electric field can be attrib-

uted to the increased distortion of the Er^{3+} site symmetry as a result of the coupling of the external electric field with the ferroelectric $BaTiO_3$ thin film.

2.2. Energy-Transfer Modulation

For an upconversion to proceed efficiently, a host lattice with low phonon energy is usually required to minimize non-radiative energy loss and maximize the radiative emission. Lanthanide-doped oxide materials with high phonon energies have limited applications owing to their low conversion efficiencies. It is well established that the transition metals with d–d transitions are able to tune the excited state properties of lanthanide ions, and subsequently have the potential to overcome the phonon quenching effect, leading to improved energy-transfer efficiency. Therefore, the incorporation of transition metals into the host lattices provides a promising route for intensified upconversion luminescence if controlled energy transfer processes can be generated. For instance, recently it has been shown by Dong et al. that the emission enhancement can reach several orders of magnitude through molybdenum (Mo^{3+}) doping in oxide host materials, including $Yb_2Ti_2O_7$, Al_2O_3, TiO_2, Gd_2O_3, and $Yb_3Al_5O_{12}$.[22] They attributed this remarkable luminescence enhancement to the efficient energy transfer from the excited state of Yb^{3+}-MoO_4^{2-} dimerized sensitizer to Er^{3+} activator. Similarly, manganese (Mn^{2+}) doping in oxide host lattices has proven effective in enhancing upconversion luminescence, especially the green emission, through sensitization of Yb^{3+}–Mn^{2+} dimer.[23]

In principle, high doping levels of activator ions (Tm^{3+}, Er^{3+}, or Ho^{3+}) acting as luminescent centers are used in UCNPs to maximize the transfer of the excitation energy absorbed by the Yb^{3+} sensitizers. However, high dopant concentrations typically lead to quenching of the luminescence due to cross-relaxation. To address this issue, Jin and co-workers[24] reported an intriguing design by applying high-power radiation fluxes onto UCNPs with high Tm^{3+} content. Using a microstructured optical fibre with a suspended-core design in which the laser excitation is confined in a micro-metre-sized core, they achieved a 70-fold enhancement in upconverted Tm^{3+} emission (Figure 4a). Importantly, the high pumping power (up to 2.5×10^6 W cm^{-2}) was able to effectively alleviate the concentration quenching effect, an optical phenomenon frequently observed under low-power excitation. The Tm^{3+} ion has four important energy states for optical transitions, labeled $^3H_6$, $^3H_5$, $^3H_4$, and $^1G_4$ (Figure 4b). When illuminated with a low-power laser, the cross-relaxation between $^1G_4 \rightarrow {}^3H_4$ and $^3H_6 \rightarrow {}^3H_5$ optical transitions is likely to cause the concentration quenching of Tm^{3+} emission from its $^1G_4$ state.[25] In contrast, a super-intense laser beam can promote the Tm^{3+} ions, located in the $^3H_4$ intermediate state through cross-relaxation, to higher lying energy levels. The synergistic effect of combined high-power excitation and cross-relaxation leads to significantly enhanced upconversion emission. It should be noted that the use of high photon fluxes in microscopy may damage biological samples unless efforts are made to limit the laser power in the focal region of the
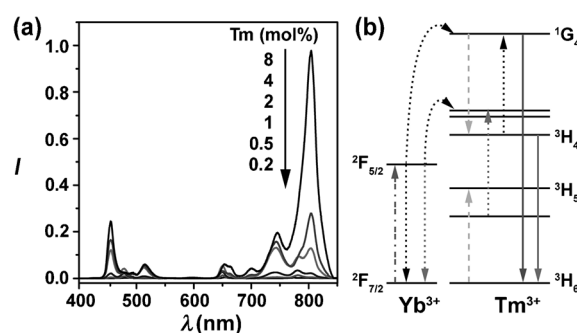

Figure 4. a) Photoluminescence spectra of $NaYF_4$:Yb/Tm nanoparticles with various Tm^{3+} concentrations under 980 nm laser excitation (2.5×10^6 W cm^{-2}) showing the Tm^{3+}-concentration dependence of upconversion emission intensity. b) Simplified energy-transfer mechanism in $NaYF_4$:Yb/Tm nanoparticles under high-density excitation. The dashed/dotted arrows = photon excitation, dotted arrows = energy transfer, dashed arrows = cross-relaxation, and full arrows = emission processes. Adapted with permission from Ref. [24]. Copyright 2013, Nature publishing group.

sample. Similarly, a high doping concentration of Yb^{3+} has also been demonstrated to enhance upconversion emission in sub 10 nm $NaLuF_4$:Yb/Tm nanocrystals. The authors ascribed the luminescence enhancement in these ultrasmall UCNPs to improved absorption and energy transfer from Yb^{3+} to Tm^{3+} despite the adverse effects of surface and concentration quenching.[26]

Host matrices can exchange excitation energy with the lanthanide dopants, leading to enhanced emission of the dopant ions at a specific wavelength. For example, the strong interaction between Mn^{2+} and Er^{3+} ions in MnF_2:Yb/Er nanocrystals can result in losses of the excitation energy at the $^4S_{3/2}$ level of Er^{3+}. This subsequently leads to increased population at the $^4F_{9/2}$ level of Er^{3+} because of energy transfer from Mn^{2+} to Er^{3+}. As a result, an enhanced intensity ratio of red-to-green emission can be obtained.[27] On the basis of these observations, we recently demonstrated a general method for the synthesis of lanthanide-doped $KMnF_3$ nanoparticles that exhibit unusual single-band upconversion emissions at approximately 660 nm on 980 nm laser excitation.[28] We showed that the absence of dopant segregation from host lattice is essential for thorough energy exchange between the dopant ion and host Mn^{2+} ion. Similar observations of single-band emission were also reported in $NaMnF_3$[29] and Mn^{2+}-doped $NaYF_4$[30] host materials. The intense single-band emission provides a promising platform for in vivo bioimaging at a substantial tissue depth.

Another notable class of host lattices capable of exchanging the excitation energy with the dopants is gadolinium-based host materials comprising optically active sublattices. Through the Gd^{3+} sublattice, the migration of the excitation energy is possible with fast rates over a long distance in favor of energy transfer process. It should be noted that the energy migration through Gd^{3+} sublattices has been broadly investigated for multicolor downconversion luminescence under a single wavelength excitation.[31] A key advantage of using Gd^{3+}-based host lattices is that the energy-migration process can permit trapping of the migrating energy by an activator ion even at a low doping level.

Despite the attractions, the generation of efficient luminescence through Gd-sublattice-mediated energy migration is generally restricted to downconversion. The challenge of upconversion in lanthanide activated systems has been met with limited success largely because of deleterious cross-relaxation between dopants and uncontrolled energy migration to defects. For upconversion to proceed, a general prerequisite for the activators is to have long-lived intermediary energy states. In 2011, our group demonstrated that by engineering a core–shell structure with a set of lanthanide ions incorporated into different layers at defined concentrations, efficient upconversion emissions can be realized through energy migration for a large array of lanthanide activators (Eu^{3+}, Tb^{3+}, Dy^{3+}, and Sm^{3+}) without long-lived intermediary energy states.[32] Equally important, we showed that the effect of energy migration through the Gd sublattice can be harnessed to provide inter-particle energy transfer to lanthanide-doped nanocrystals as energy acceptors. This optical phenomenon is striking, considering that lanthanide-doped nanocrystals have been rarely used as acceptors for Förster resonance energy transfer (FRET) studies due to their significantly narrow absorption cross sections (ca. 10^{-21} cm^2).

To prevent the surface quenching of the migrating energy, our group further developed a core–shell–shell strategy with an optically inert $NaYF_4$ layer grown onto the lanthanide-doped $NaGdF_4$:Yb/Tm@NaGdF_4$:A nanoparticle (Figure 5 a,b).[33] We showed that substantially enhanced upconversion emission through energy migration could be achieved

by this multilayered core–shell design. More importantly, the $NaYF_4$ shell-coating strategy enabled tunable optical emissions for the activators doped at very low concentrations (down to 1 mol % for Dy^{3+}, Sm^{3+}, Tb^{3+} and Eu^{3+}; Figure 5 c).[33]

To enhance luminescence intensity in lanthanide-doped UCNPs, an increased level of doping by the Yb^{3+} sensitizer is typically required for achieving practically useful upconversion emission. However, high levels of Yb^{3+} (typically greater than 20 mol %) in conventional nanocrystals can lead to immense quenching of luminescence owing to an increased probability of random energy migration to lattice or surface defects (Figure 6 a). Therefore, efficient preservation and utilization of the excitation energy play a key role in improving energy-transfer efficiency. Our group recently demonstrated a new class of orthorhombic KYb_2F_7:Er (2 mol %) nanocrystals with Yb^{3+} ions arranged in tetrad clusters.[34] This lattice arrangement effectively minimizes the migration of excitation energy (Figure 6 b), resulting in an unusual four-photon-promoted violet upconversion emission at 410 nm with an intensity more than eight-times higher than previously reported (Figure 6 c).

2.3. Surface Passivation

When compared with their bulk counterparts, lanthanide-doped UCNPs often suffer from much stronger surface quenching effects owing to their high surface-to-volume ratio.
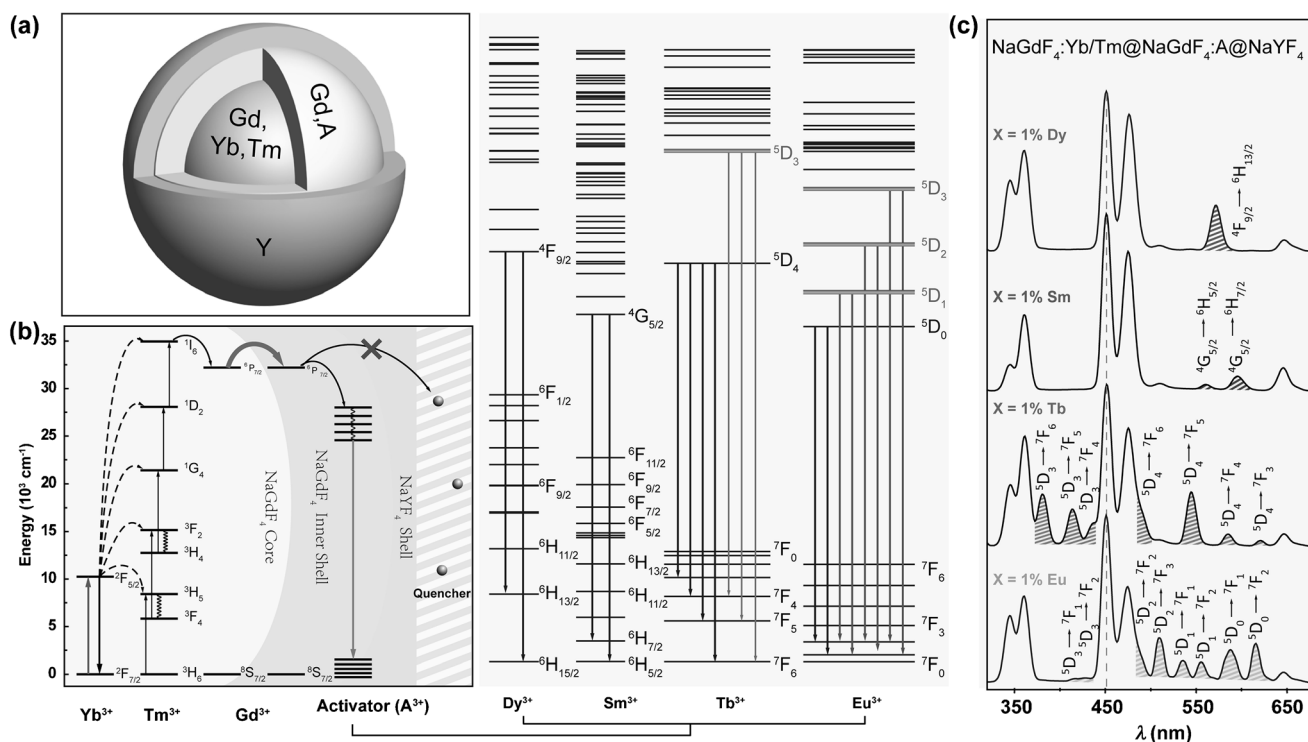

Figure 5. Energy-migration-mediated upconversion (EMU) in core–shell–shell nanoparticles. a) Schematic design of a lanthanide-doped NaGdF$_4$:Yb/Tm@NaGdF$_4$:A @NaYF$_4$ nanoparticle for EMU (A=activator ion). b) Proposed energy-transfer mechanisms in the multi-layered nanoparticle. c) Room-temperature emission spectra of the NaGdF$_4$:Yb/Tm@NaGdF$_4$:A@NaYF$_4$ nanoparticles with 1% of activator concentration. Adapted with permission from Ref. [33]. Copyright 2012, American Chemical Society.

11706 www.angewandte.org

© 2014 Wiley-VCH Verlag GmbH & Co. KGaA, Weinheim

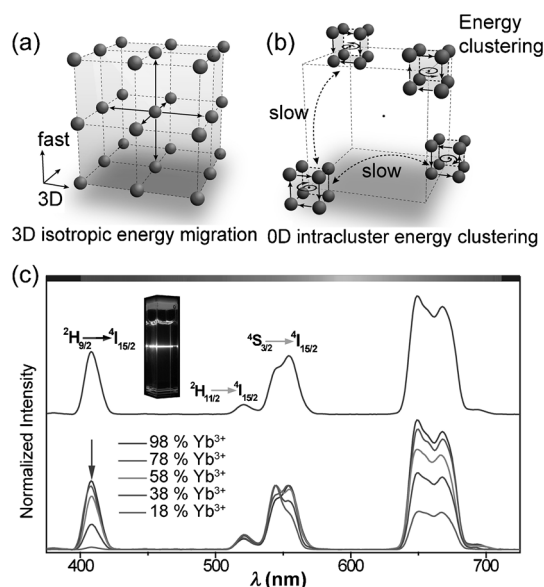*Angew. Chem. Int. Ed.* **2014**, *53*, 11702–11715

Figure 6. Schematic representation showing two different types of crystal sublattice: a) 3D isotropic energy migration and b) 0D intra-cluster energy clustering. The migration of excitation energy can be effectively minimized by the energy clustering in discrete sublattices. c) The upconversion emission spectra of KYb$_2$F$_7$:Er (2 mol%) (top) and KYb$_2$F$_7$:Er/Lu (2/0–80 mol%) (bottom) nanoparticles obtained under a 980 nm laser excitation. Inset: a typical photograph of KYb$_2$F$_7$:Er nanocrystals. Adapted with permission from Ref. [34]. Copyright 2014, Nature publishing group.

This is particularly true for small-sized nanoparticles in which surface-related effects dominate the energy-loss mechanism. Lanthanide-doping processes in these nanoparticles are always accompanied by the trapping of a large portion of dopant ions on the outermost layer of the nanoparticles (Figure 7a). Therefore, the luminescence of the surface
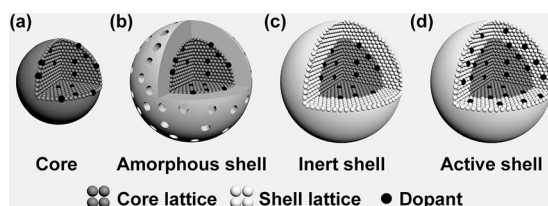

Figure 7. Schematic illustrations of different types of core–shell structure for enhanced upconversion luminescence. a) Lanthanide-doped core nanoparticle. b) Amorphous shell coating. c) Inert crystalline shell coating. d) Active-shell design with sensitizers or activators doped in the shell layer.

dopants can be readily quenched by high-energy oscillators arising from surface impurities, ligands, and solvent molecules through multi-phonon relaxation processes. Additionally, the excitation energy carried by the interior ions is likely to be transferred to the surface quenching sites, resulting in non-radiative relaxation.

The overall de-activation rate constant (k_{obs}) at a specific temperature (T) is described by Equations (1):

$$k_{obs} = k^r + \sum_n k_n^{nr}$$

$$\sum_n k_n^{nr} = \sum_i k_i^{vib}(T) + \sum_j k_j^{et}(T) + \sum_k k_k^{'nr} \tag{1}$$

where k^r and k^{nr} are the radiative and non-radiative rate constants, respectively. Note that k^{nr} is the sum of the non-radiative rate constants associated with vibrational processes (k^{vib}), photoinduced energy-transfer processes (k^{et}), and the remaining deactivation paths ($k^{'nr}$).[35] In lanthanide-doped UCNPs, the vibration-induced non-radiative process caused by the surface quenching effect is mainly responsible for low values of upconversion efficiencies. Surface passivation through a conformal shell coating onto the nanoparticle offers an effective strategy to tune the energy transfer between the dopants. More importantly, through the core–shell design all dopant ions can be spatially confined in the interior core of the nanoparticle, thereby suppressing the surface-dopant-induced quenching of excitation energy.

Amorphous shell coating is a convenient approach for increasing the efficiency of the energy-conversion process (Figure 7b). Several studies have explored the effect of amorphous shell coating on the luminescence properties of UCNPs. For example, Lü et al. coated Y$_2$O$_3$:Yb/Tm nanoparticles with a non-crystalline silica (or titania) layer. They found that the emission intensity of the nanoparticles can be controlled by varying the thickness of the silica shell.[36] In another demonstration, Li et al. reported the enhancement of upconversion luminescence in NaYF$_4$:Yb/Er nanoparticles by carbon shell coating. In comparison with silica-coated analogues with a similar shell thickness, the carbon-coated UCNPs exhibited much stronger emission intensities.[37]

The utilization of an optically inactive crystalline shell having the same composition as the host lattice not only provides a strong crystal field, but also effectively prevents the transfer of excitation energy to the particle surface (Figure 7c). Yi and Chow investigated the crystalline-shell-coating effect in 8 nm NaYF$_4$:Yb/Tm nanocrystals coated with a 1.5 nm-thick NaYF$_4$ shell. Interestingly, they observed a nearly 30-fold enhancement of the upconversion luminescence.[38] This approach could be extended with reasonably good success to enhance the luminescence in other host materials.[39] Notably, our group recently achieved a more than 450-fold increase in the emission intensity for 10 nm NaGdF$_4$:Yb/Tm nanoparticles upon surface coating with a 2.5 nm thick NaGdF$_4$ shell.[40]

Dopant diffusion at elevated temperatures is likely to occur at the core–shell interface during the shell-growth step. To give the nanoparticle improved thermal stability, a crystalline shell with a material composition different from the core can be considered. Yan and co-workers have demonstrated that the coating of CaF$_2$ shell onto α-NaYF$_4$:Yb/Er nanoparticles can markedly enhance upconversion emission.[41] The photoluminescence of NaYF$_4$:Yb/Er@CaF$_2$ nanoparticles can be enhanced by a factor of 4 to 5 compared to NaYF$_4$:Yb/Er@NaYF$_4$ nanoparticles of a similar size. In a parallel development, Chen et al. reported a 35-fold increase in the NIR emission of α-NaYbF$_4$:Tm@CaF$_2$ core–shell nanoparticles.[42]

As an active shell with intentionally added dopants combines the benefit of a suppressed surface-quenching effect with an increased capacity for high-level doping, they can offer attractive optical properties not accessible by other types of core–shell structures (Figure 7d). In 2009, Capobianco and co-workers reported the enhancement of upconversion emission in NaGdF$_4$:Yb/Er nanoparticles coated with a thin NaGdF$_4$:Yb shell (Figure 8a).[43] This Yb^{3+}-modified
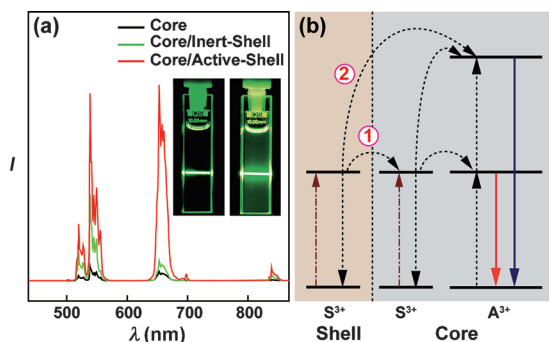

Figure 8. a) Upconversion luminescence spectra of NaGdF$_4$:Yb/Er core, NaGdF$_4$:Yb/Er@NaGdF$_4$ (core/inert shell) and NaGdF$_4$:Yb/Er@-NaGdF$_4$:Yb (core/active shell) nanoparticles under the excitation of a 980 nm laser. Inset: the corresponding photos of these UCNP solutions. b) Proposed energy-transfer mechanism showing the possible pathways responsible for emission enhancement in an UCNP coated with a sensitizer-doped active shell. Pathway 1: A sensitizer ion (S^{3+}) doped in the shell layers absorbs the excitation energy, followed by the migration of excitation energy through the neighboring sensitizers through the core–shell interface. Subsequently, the migrating energy is trapped by an activator ion (A^{3+}). Pathway 2: A sensitizer ion in the shell layer can absorb the excitation energy and directly transfer it to the activator ion in the core layer. The dashed/dotted arrows = photon excitation, dotted arrows = energy transfer, and full arrows = emission processes. Adapted with permission from Ref. [43].

shell allows the preservation of excitation energy and efficient energy transfer to the activators confined in the core structure (Figure 8b). In two independent follow-up studies, Lin and co-workers and Tsang and co-workers reported the observation of active-shell-induced luminescence enhancement in BaGdF$_5$@BaGdF$_5$:Yb and CaF$_2$@NaYF$_4$:Yb core–shell nanocrystals, respectively.[44]

In addition to sensitizer-encapsulated shells, the active shell modification with activators can also be used to enhance emission intensity and empower fine tuning of upconversion emission. For example, Zhang and Qian[45] reported NaYF$_4$@NaYF$_4$ core–shell nanocrystals doped with Yb^{3+}/Tm^{3+} and Yb^{3+}/Er^{3+} into the core and shell layer, respectively. Using a similar strategy, Liu et al.[46] achieved significantly enhanced emission of Er^{3+} in NaYF$_4$-based multi-layered nanocrystals. They found that the upper limit of the concentration quenching threshold for Er^{3+} activator was improved from around 2 mol% to 5 mol%.

In 2010, this active shell strategy was explored by Chen and co-workers[47] to demonstrate dual-modal emissions in NaGdF$_4$:Yb/Tm@NaGdF$_4$:Eu core–shell nanocrystals. The advantage of using NaGdF$_4$:Eu active shell is that it allows them to enhance upconversion luminescence of the NaGd-

F$_4$:Yb/Tm core while the downshifting luminescence of Eu^{3+} is not compromised. In a recent study, Wang and co-workers[48] came up with a recipe to synthesize sub-10 nm BaF$_2$:Yb/Tm@SrF$_2$:Gd/Nd nanocrystals comprising a hetero-core–shell nanostructure. Importantly, the upconversion emission of Yb^{3+}/Tm^{3+} couple and downshifting emission from Nd^{3+} and Yb^{3+} ions were both located in the NIR window, also known as optical or therapeutic window, where light has its maximum depth of penetration in tissue. These characteristics in combination with the magnetic properties of Gd^{3+} make BaF$_2$:Yb/Tm@SrF$_2$:Gd/Nd nanocrystals an excellent candidate as multi-modal probe for medical imaging and diagnosis.

2.4. Surface-Plasmon Coupling

Noble-metal nanoparticles have gained much interest in recent years owing to their strong light absorption and scattering, particularly in the visible region. Localized surface-plasmon resonance can occur in metal nanoparticles in which confined free electrons oscillate at frequencies similar to those of passing photons and subsequently enter resonance. Surface plasmons are able to propagate along a metallic surface and give rise to intense electromagnetic fields. Consequently, metal nanoparticles have been proposed as effective light-trapping component that can be coupled with UCNPs to boost the efficiency of the energy conversion process.

The intensity (I) of upconversion emission in a typical lanthanide-doped nanocrystal can be estimated by Equation (2):

$$I = \phi \cdot \sigma_S \cdot \eta_{ET} \cdot \varphi_A \tag{2}$$

Where, ϕ is the photon flux of the incident radiation, σ_S is the absorption cross section of the sensitizer ion (Note: The absorption by the activator ion is neglected because of its very small absorption cross section.), η_{ET} is the energy-transfer efficiency from the sensitizer to the activator, and φ_A is the luminescence quantum yield of the activator.

The surface plasmon can greatly influence the luminescence of UCNPs in three ways:[49] 1) enhancing the absorption of the sensitizer through electric-field coupling, 2) improving the radiative decay rate of the activator, and 3) increasing energy transfer from the sensitizer to the activator (Figure 9).

The strong local electric field (E) induced by surface-plasmon resonance may enhance the photon flux (ϕ) of the excitation, which is proportional to the square of the electric field as described in Equation (3):

$$\phi \propto |E|^2 \tag{3}$$

Hence, when an UCNP is placed in the vicinity of a metal nanoparticle, an improved light harvesting by sensitizer ions as a result of an effective coupling between the electric field of the plasmon with the transition dipole of the UCNP can be expected, thereby leading to enhanced upconversion luminescence.[50]
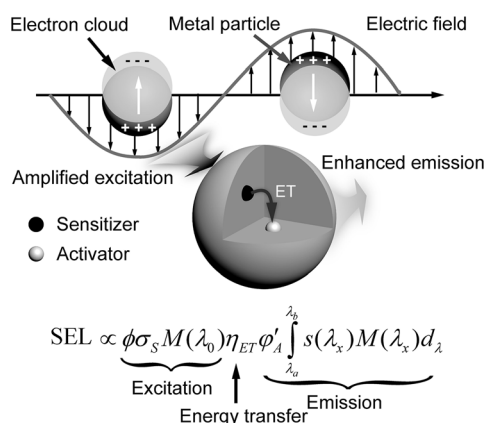
11708   www.angewandte.org

© 2014 Wiley-VCH Verlag GmbH & Co. KGaA, Weinheim

Angew. Chem. Int. Ed. **2014**, *53*, 11702 – 11715

Figure 9. Schematic illustration showing the plausible mechanism that governs the plasmonic enhancement of upconversion luminescence. Note that surface plasmon-enhanced luminescence (SEL) depends on various factors including the photon flux of the excitation (ϕ), absorption cross section (σ_S) of the sensitizer, field enhancement factor (M), energy-transfer efficiency from the sensitizer to the activator (η_{ET}), quantum yield (φ_A) of the activator, and the relative emission function $s(\lambda_x)$.

A great deal of coupling occurring between the electrons and phonons in a metal nanoparticle can also change the radiative decay rate of the activator doped in an UCNP, which modifies the photonic-mode density of upconverted luminescence. Therefore, the quantum yield (φ_A) and observed luminescence lifetime (τ) can be calculated using Equations (4) and (5), respectively:

$$\varphi_A = \frac{k_r + k_m}{k_r + k_m + k_{nr}} \qquad (4)$$

$$\tau = \frac{1}{k_r + k_m + k_{nr}} \qquad (5)$$

where k_r, k_{nr}, and k_m are the radiative decay rate, non-radiative decay rate, metal-induced additional radiative decay rate, respectively. If the UCNP and the metal nanoparticle are placed within the range of 5 nm to one another, direct electron transfer or FRET can occur and thus quench the luminescence. To obtain enhanced quantum efficiency, a minimum spacing of 5 nm is generally needed between these two types of optical materials for the advantages of decreased non-radiative and increased radiative decay rates to be apparent.[51]

The surface-plasmon resonance strongly depends on the size, shape, and composition of the metal substrate. Therefore, the optimization of plasmonic structure is of great significance for enhancing upconversion luminescence. Early studies often focused exclusively on spherical Ag particles embedded with lanthanides in amorphous matrices.[52] Recently, the effect of surface plasmons on upconversion has been investigated in a number of studies involving Ag nanowires,[53] single Au nanoparticles,[54] and Au island films,[55] with the enhancement factors of up to 5.

Paudel et al.[56] have shown how conversion efficiency can be largely boosted using lithographically patterned nano-

pillars on Au substrates. The plasma frequency of the substrate consisting of Au nanoarrays matched well with the excitation frequency. Their finite-difference time-domain simulation (FDTD) revealed that this lithographically engineered substrate could provide an approximately 11-fold amplification on excitation intensity when compared to a smooth Au thin film substrate. In 2012, Saboktakin et al.[57] reported the enhancement of upconversion luminescence through use of a metal/oxide/upconversion multi-layered structure. They systematically investigated the dependence of the luminescence enhancement on the thickness of the oxide layer and the type of metal nanoparticles. Maximum enhancement factors of 5.2 and 45 were achieved for Au and Ag nanoparticles, respectively (Figure 10a). One year later,
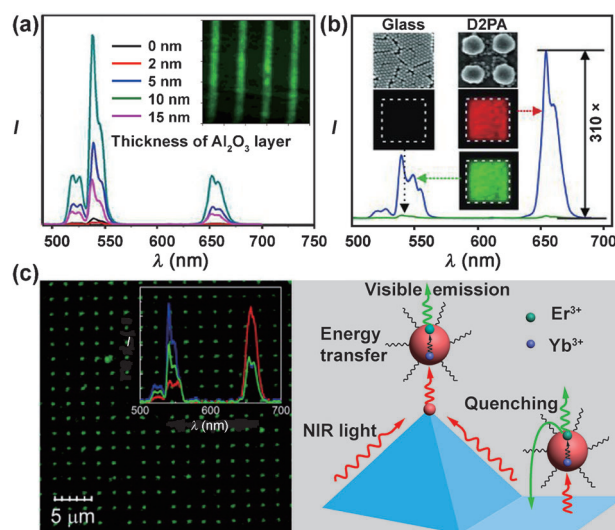

Figure 10. Selected forms of lithographically patterned plasmonic arrays for enhanced upconversion luminescence. a) Green emission enhancement in patterned Au/Al$_2$O$_3$/NaYF$_4$:Yb/Er thin films. b) Luminescence enhancement in the green (550 nm) and red (660 nm) emission through use of a disk-coupled dot-on-pillar antenna array (D2PA). c) Upconversion emission enhancement using NaYF$_4$:Yb/Er particles coupled with patterned gold pyramids. Left: the confocal image Inset: corresponding emission spectra of the patterned nanostructures. Right: simplified schematic representation of the energy-transfer, upconversion, and quenching processes taking place in the hybrid system. Adapted with permission from Ref. [57] (Copyright 2012, American Chemical Society),Ref. [59], and Ref. [60] (Copyright 2014, American Chemical Society).

the same group designed Au nanohole arrays that enabled frequency-dependent luminescence enhancement of up to 35-fold.[58]

Under the resonant condition, a considerable increase in the excitation field could provide a large enhancement in upconversion luminescence. An excellent example was demonstrated in 2012 by Chou and co-workers,[59] who deliberately designed a 3D plasmonic nanoantenna architecture consisting of periodic SiO$_2$ pillars encapsulated with different types of Au nanostructures. The plasma frequency could be tuned by varying the height of the SiO$_2$ pillars. When the resonant-absorption peak was tuned at approximately 920 nm

with an optimal pillar height of 75 nm, a remarkable 310-fold luminescence enhancement over a large area was observed (Figure 10 b).
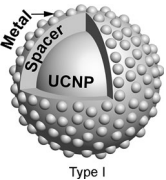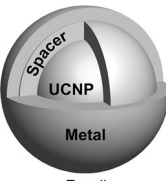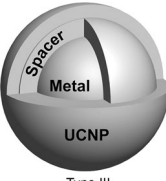
Apart from the excitation-field enhancement and improvement over the radiative decay rate, surface-plasmon coupling can alter the rate of energy transfer from the sensitizer to activator ions. To test this idea, Nagpal and coworkers[60] reported a 6-fold rate amplification in the energy transfer from Yb^{3+} to Er^{3+} using gold pyramid arrays (Figure 10 c). By comparing the experimental results obtained from the glass, flat Au, and as-prepared Au pyramid substrates, they successfully decoupled different effects of patterned metal nanostructures on upconversion emission, including electromagnetic field, quenching, and energy-transfer dynamics.

As in the plasmonic arrays, there is evidence that core–shell UCNPs modified with noble metals may also lead to enhanced upconversion luminescence. The core–shell design is more feasible for biological applications in which control of particle dispersion is essential. The plasmon-enhanced UCNPs adopting core–shell structures can be broadly classified into three categories: UCNP-core/polymer-shell (or silica-shell) systems decorated with metal nanoparticles (Type I), UCNP-core/silica-shell/metal-shell systems (Type II), and metal-core/silica-shell/UCNP-shell systems (Type III). Table 1 summarizes the basic structural design, common building blocks, and enhancement factors of the above-mentioned three categories.

It is important to note that the metal-shell design (Types I and II) may cause a decrease in the light absorption by the UCNP core because of the scattering and absorption that occurs for plasmonics. In addition, under direct and prolonged light irradiation, the thermal stability of the metal shell becomes a crucial issue, which often leads to poor optical performance. By comparison, the metal-core configuration (Type III) is designed for maximum light absorption by the UCNP shell and flexible control over the size of the metal core. As an added benefit, the thickness of the spacer layer that separates the metal core from the UCNP shell can be conveniently controlled to achieve an optimized plasmonic enhancement effect. In 2010, Zhang et al.[61] made the case that an optimized spacer thickness in $Ag@SiO_2@Y_2O_3$:Er nanoparticles can lead to a maximum emission enhancement factor of 4. In 2013, Ge et al.[62] also demonstrated the feasibility of using the metal-core configuration for upconversion luminescence enhancement. In their report, the green emission (ca. 549 nm) of $Au@SiO_2@Y_2O_3$:Yb/Er nanoparticles was enhanced 9.5-fold using a 30 nm Au core.

The shape of active plasmonic nanostructures can also be tailored to provide precise control over upconversion luminescence. It is well established that spherical Au nanoparticles exhibit a single plasmon band, whereas structures such as nanorods exhibit two characteristic peaks corresponding to longitudinal and transverse modes. Critically, the longitudinal mode allows the optical absorption range to be extended to the NIR region. Thus, the longitudinal mode can be effec-

Table 1: Current developments for plasmonic enhancement of upconversion luminescence.

Structure Design	Core (size)	Building Block Spacer[a] (size)	Shell (size)	Enhancement Factor (Emission wavelength)	Ref.
Type I	$NaYF_4$:Yb/Tm	PAA/PAH	Au (2 nm)	≈ 2.5 (452 nm, 476 nm)	[64]
	$NaYF_4$:Yb/Er/Gd	–	Au sphere	3.8 (540 nm); 4.0 (660 nm)	[65]
	$NaYF_4$:Yb/Er	SiO_2 (10 nm)	Ag (15 nm)	14.4 (542 nm); 12.2 (656 nm)	[66]
			Ag (30 nm)	9.5 (542 nm); 10.8 (656 nm)	
	$NaYF_4$:Yb/Tm	–	Au (≈ 10 nm)	73.7 (291 nm); 109.0 (345 nm); 44.9 (362 nm); 49.8 (450 nm); 29.9 (474 nm)	[67]
	$NaYF_4$:Yb/Tm	PAMAM (2.5 nm)	Au rod	27 (805 nm); 6 (470, 550 nm)	[68]
	$NaYF_4$:Yb/Er	SiO_2 (11 nm)	Ag sphere	4.4 (525 nm, 545 nm); 3.5 (660 nm)	[69]
Type II	$NaYF_4$:Yb/Er	SiO_2 (11 nm)	Au shell	9.1 (525 nm, 545 nm); 6.75 (660 nm)	[69]
	$NaYF_4$:Yb/Er/Gd	–	Au shell	3.2 (540 nm); 9.6 (660 nm)	[65]
	$NaYF_4$:Yb/Er/Tm	–	Au shell (4–8 nm)	8 (646 nm)	[70]
	$NaYF_4$:Yb/Er	SiO_2 (18 nm)	Au shell (2.8 nm)	≈ 4 (410 nm); ≈ 2.6 (545 nm); ≈ 2.3 (660 nm)	[71]
	$NaYF_4$:Yb/Er/Tm	PAMAM	Au shell (20 nm)	20 (518 nm); 21 (540 nm)	[72]
			Ag shell (20 nm)	20 (413 nm); 22 (452 nm)	
Type III	Ag (130 nm)	SiO_2 (20 nm)	Y_2O_3:Er	3.86 (550 nm); 3.39 (650 nm)	[61]
	Ag (50 nm)	SiO_2 (40 nm)		4.37 (550 nm); 3.06 (650 nm)	
	Ag (50 nm)	SiO_2 (30 nm)		4.76 (550 nm); 3.26 (650 nm)	
	Ag (20 nm)	SiO_2 (35 nm)		1.77 (550 nm); 2.08 (650 nm)	
	Au (30 nm)	SiO_2 (25 nm)	Y_2O_3:Yb/Er (12 nm)	1.51 (549 nm)	[62]
		SiO_2 (30 nm)		2.14 (549 nm)	
		SiO_2 (40 nm)		9.59 (549 nm)	
		SiO_2 (45 nm)		3.51 (549 nm)	
	Au nanorod	SiO_2	LaF_3:Yb/Er	6.5 (550 nm)	[63]

[a] PAA: Poly(acrylic acid); PAH: Poly(allylamine hydrochloride); PAMAM: Polyamidoamine dendrimer.

tively coupled to commonly used 800 nm or 980 nm excitation sources for luminescence enhancement. Zhang and Lee[63] validated this hypothesis in Au@SiO$_2$@LaF$_3$:Yb/Er core–shell nanostructures featuring Au nanorods with average aspect ratios of 3–4. Interestingly, they observed a 6.5-fold enhancement of Er^{3+} emission at 550 nm through use of the Au nanorods.

2.5. Broadband Sensitization

Surface passivation and surface-plasmon coupling have proven effective in enhancing upconversion luminescence. However, the limitation inherent to the conventionally used 980 nm laser sources needs to be addressed to make upconversion nanomaterials useful. For imaging of biological systems, the 980 nm laser excitation often causes strong water absorption and thus sample overheating, which can result in cell and tissue damage. For applications in photovoltaics, upconverters capable of absorbing photons covering a wide spectral range are needed for high conversion efficiency. Recently, considerable efforts have been devoted to developing novel nanoparticles featuring broadband NIR absorption.

An ideal broadband spectral sensitizer for photon upconversion should meet the following criteria: wide bandwidth characteristics of the excitation spectrum, low density of energy states in the visible to minimize the probability of back energy transfer from the activator to sensitizer, weak coupling of the excitation energy level with lattice phonons, and a large energy gap to the next lower level to minimize the non-radiative cross-relaxation.[76]

Incorporation of two different sensitizers into a nanoparticle is an easy way to expand the excitation spectrum. Table 2 lists typical NIR spectral sensitizers used for upconversion. Er^{3+} and Ho^{3+} ions have strong absorptions in the range 1480–1600 nm ($^4I_{15/2} \rightarrow ^4I_{13/2}$ transition) and 1140–1250 nm ($^5I_8 \rightarrow ^5I_6$ transition), respectively. Both absorption ranges are transparent to crystalline-silicon (c-Si) solar cells. Upon photon upconversion, the particle emission matches well with the absorption of c-Si ($E_g = 1.1$ eV). This upconversion strategy provides an effective solution to thermalization and loss of sub-bandgap light in c-Si solar cells. An intriguing proof-of-principle example was demonstrated by Wang and co-workers,[77] who examined a series of NaGd-F$_4$:Er@NaGdF$_4$:Ho@NaGdF$_4$ core–shell–shell nanoparticles. In their design, Er^{3+} and Ho^{3+} ions were doped into the core and inner shell layer, respectively. This core–shell design effectively suppressed the adverse energy transfer between the two sensitizers while maximizing light absorption in the NIR range (Figure 11).

The conventional UCNP-based technique has made high-contrast biological imaging possible through the elimination of autofluorescence, but it requires the development of suitable particle systems which can be excited by 800 nm lasers to minimize the overheating effect associated with 980 nm excitation. In 2011, Andersson-Engels and co-workers[78] reported in vitro and in vivo bioimaging without overheating problems by using 915 nm-excitable NaYbF$_4$:Tm/Er/Ho UCNPs. They also demonstrated that the 915 nm laser is

Table 2: Typical upconversion sensitizers used in nanoparticles for transferring the energy of absorbed light to lanthanide activators.

Sensitizer	Main absorption wavelength [nm][a]	Excitation transition	Activators[b] Er^{3+}	Tm^{3+}	Ho^{3+}	Absorption cross section [cm^2]	Ref.
Yb^{3+}	980	$^2F_{7/2} \rightarrow ^2F_{5/2}$	+	+	+	$\approx 10^{-20}$	[73]
Nd^{3+}	730, 808, and 865	$^4I_{9/2} \rightarrow ^4F_{7/2},\ ^4F_{5/2},\ ^4F_{3/2}$	+	+	+	$\approx 10^{-19}$	[74]
Er^{3+}	1480–1600	$^4I_{15/2} \rightarrow ^4I_{13/2}$	+			$\approx 10^{-21}$	[75]
Ho^{3+}	1140–1250	$^5I_8 \rightarrow ^5I_6$			+	$\approx 10^{-21}$	[5a]

[a] Absorption wavelength may change in different host matrices. [b] +: sensitized upconversion. Note that for efficient upconversion to proceed, Yb^{3+} is generally co-doped for Nd^{3+}-sensitized upconversion.
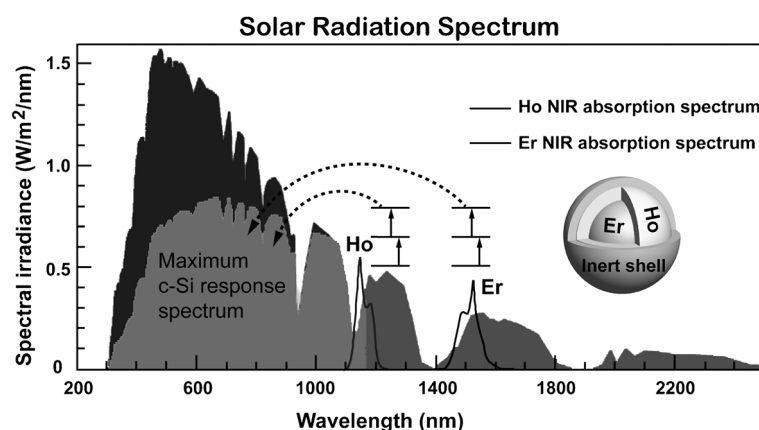

Figure 11. Schematic illustration of Er^{3+} and Ho^{3+} co-sensitized UCNPs designed to improve optical response of c-Si solar cells to NIR light. Adapted with permission from Ref. [77]. Copyright 2012, Royal Society of Chemistry.
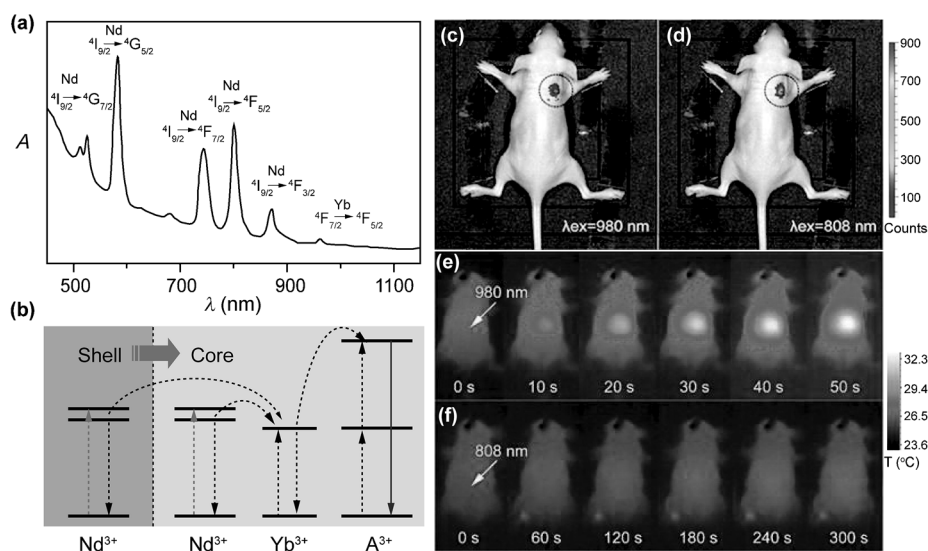
Figure 12. a) Absorption spectrum of $NaGdF_4$:Yb/Er@$NaYF_4$:Nd/Yb nanoparticles. b) Proposed Nd^{3+}-sensitized upconversion mechanism in core–shell nanoparticle under 800 nm excitation. Note that A^{3+} refers to activator ion. c,d) In vivo upconversion images (marked by circles) of a nude mouse injected with $NaGdF_4$:Yb/Er@$NaYF_4$:Nd/Yb nanoparticles and under the 980 nm and 808 nm laser irradiation, respectively. e,f) In vivo heating effects induced by the irradiation of two laser sources as a function of exposure time. Adapted with permission from Refs. [73] (Copyright 2013, American Chemical Society), and [81] (Copyright 2013, American Chemical Society).

superior to the 980 nm counterpart for deep tissue imaging. Two years later, Han and co-workers[79] took one step further and reported Nd^{3+}-based nanoparticles excitable by an 800 nm laser. This 800 nm laser excitation is ideal for biological imaging because of the low absorption coefficients of many biological specimens and water at this wavelength. It is also worth noting that Nd^{3+} has two additional NIR absorption bands at 730 nm and 865 nm, in addition to the strong absorption peak at 800 nm (Figure 12 a).[73,80]

In the aforementioned Nd^{3+}-sensitized upconversion, the doping level of Nd^{3+} has to be kept very low (typically under 2 mol%) to minimize deleterious cross-relaxation between the Nd^{3+} and the activator ions. To overcome this problem, our group introduced a rational core–shell strategy that enabled high-concentration doping (20 mol%) of Nd^{3+} and markedly enhanced upconversion emission under 800 nm excitation (Figure 12 b).[81] Using this active-shell strategy, we achieved emission intensity approximately 7 times higher than that obtained with an inert $NaYF_4$ shell. In a parallel investigation, Yan and co-workers[73] also reported intense Nd^{3+}-sensitized upconversion luminescence in $NaGdF_4$:Yb/Er@$NaGdF_4$:Nd/Yb core–shell nanoparticles. Interestingly, the use of the Nd^{3+}-based UCNPs showed comparable efficacy for in vivo bioimaging to Yb^{3+}-based particles when irradiated at 808 nm and 980 nm, respectively (Figure 12 c,d). Notably, the mice exposed to 808 nm laser over a period of 5 min did not show a noticeable heating effect as opposed to the control group excited with 980 nm laser (Figure 12 e,f). The potential benefit of Nd^{3+}-sensitized upconversion in nanoparticles for prolonged imaging without overheating the biological samples has also been validated by several other research groups.[82] Together, these efforts reveal important features about the incorporation and organization of Nd^{3+}

ions in UCNPs and shed light on more efficient multiphoton access to the infrared region.

Alternatively, organic dyes can be used as broadband sensitizers for enhanced upconversion luminescence owing to their large absorption cross sections. Zou et al.[83] showed that the utilization of a carboxylic acid-modified cyanine dye enabled a broadband excitation of $NaYF_4$ nanoparticles co-doped with Yb^{3+} sensitizers and Er^{3+} activator ions. In their design, the cyanine dye, placed in close proximity to the nanoparticle, acts as an antenna to absorb packets of optical energies across a broad wavelength range (740–850 nm) and then transfers this energy to Yb^{3+} ions trapped in the host lattice through a FRET process. Over a spectral range from 720 nm to 1000 nm, the dye-sensitized nanoparticles showed a remarkable 3300-fold increase in luminescence intensity as a result of increased absorptivity and overall broadening of the absorption spectrum of the nanoparticles.

2.6. Photonic-Crystal Engineering

Photonic crystals, made from artificial periodic patterns of materials with different permittivities, have been recently explored as promising alternatives to enhance upconversion luminescence. Light can be trapped in photonic crystals with an enhanced density of optical states and then guided to interact with UCNPs. Through resonance of the input frequency with photonic crystal modes, increased electric-field intensity can be anticipated, leading to amplified absorption of the nanoparticles at the resonant frequency.

Song and co-workers[84] examined the effect of adding $NaYF_4$:Yb/Tm/Er UCNPs to photonic crystals based on polymethyl methacrylate (PMMA) opals (Figure 13 a,b). This
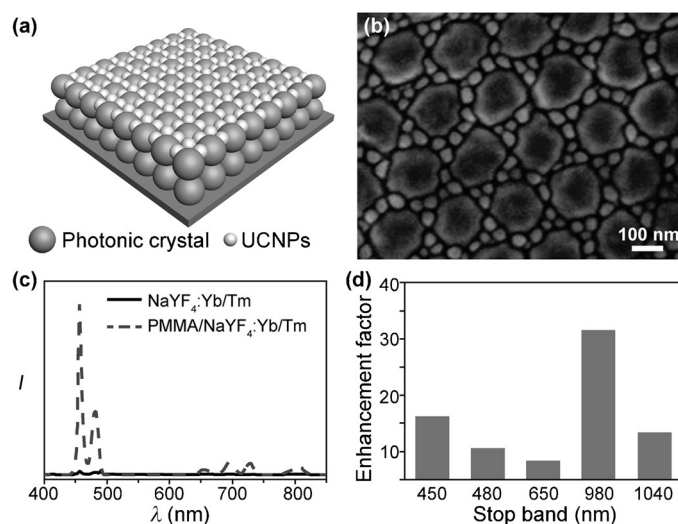
Figure 13. a) Schematic representation of photonic crystals filled with UCNPs. b) SEM image of the as-synthesized PMMA structure with NaYF$_4$:Yb/Tm nanoparticles filled in the pores. c) Upconversion emission spectra obtained with and without the PMMA opals. d) The upconversion enhancement factors as a function of the photonic stop band of PMMA opals. Adapted with permission from Ref. [84]. Copyright 2013, Royal Society of Chemistry.

carefully designed system can yield a maximum achievable intensity 32 times higher than the unstructured nanoparticles (Figure 13 c). They found that the degree of the enhancement strongly depends on the stop band of photonic crystals. A maximum luminescence improvement was achieved when the excitation frequency matched well with the stop band (Figure 13 d). Yang and co-workers[85] also demonstrated that Yb^{3+}/Er^{3+} or Yb^{3+}/Tm^{3+} co-doped NaYF$_4$ nanoparticles, resting on polystyrene-based photonic crystals, can boost upconversion emission intensity. Mechanistic studies led to the suggestion that the Bragg reflection of the photonic crystals and the close match of the photonic bandgap to the emission wavelength are major contributors to the improved luminescence. Very recently, Niu et al.[86] developed an interesting method for using photonic crystals to increase the fraction of incoming light absorbed by NaYF$_4$:Yb/Tm nanoparticles. Their materials comprised a structured polystyrene frame filled with a periodic arrangement of air pores. The nanoparticles sat on the surface of the pores. In accord with design expectations, much higher emission intensity was observed with the hybrid materials than the same experiment performed with the nanoparticles alone. The researchers further fabricated a carbon nanotube-based phototransistor designed specifically to take advantage of the upconversion photonic crystals. The device showed a 10-fold increase in photoresponsivity in the NIR range.

3. Summary and Outlook

By reviewing the recent efforts to enhance luminescence in lanthanide-doped UCNPs, it is clear that significant progress has been made in terms of understanding lanthanide

photochemistry and the control of light at nanoscale dimensions. Importantly, these efforts have led to novel nanomaterials with extraordinary optical properties that can provide solutions to a broad range of pressing scientific and technological challenges. Particularly, the ability of these nanomaterials to release high-energy photons after NIR laser-light stimulation allows deep tissue imaging and in vivo biological application, a feat hardly accessible by conventional contrast agents or luminescent nanoparticles. Great imaging depth is achieved by optimum harvesting of incident photons, accompanied by highly efficient upconversion processes. As we gain unprecedented control over spatially confined lanthanide dopants, entirely new optical phenomena are also possible.

Despite the enticing prospects of UCNPs, there are a number of significant challenges facing materials chemists. For instance, further experiments and theoretical works are needed to sort out the detailed mechanisms of energy transfer in these nanoparticles, and the major drawbacks associated with low efficiency of current lanthanide-doped upconverters. The question remains open as to whether the excitation of UCNPs can be realized with relatively low power density (ca. a few mW cm^{-2}).

A thorough answer to these questions will require a better understanding of the spatial distribution of lanthanides within the nanoparticle. Additional characterization techniques need to be developed to reveal the precise concentration of dopant ions at single-particle levels. Recent investigations on ultrasmall single UCNPs may constitute an important step towards a deeper understanding of the effect of lanthanide doping.[87] On another matter, instead of obsessing over improved performance from common lanthanide activators, more attention might be given to looking for replacements with comparable performance. Nonetheless, we believe that lanthanide-doped UCNPs will have broad utility in fundamental research and many technological applications.

[1] a) F. Auzel, *Chem. Rev.* **2004**, *104*, 139–174; b) F. Wang, Y. Han, C. S. Lim, Y. Lu, J. Wang, J. Xu, H. Chen, C. Zhang, M. Hong, X. Liu, *Nature* **2010**, *463*, 1061–1065; c) J. Zhou, Z. Liu, F. Li, *Chem. Soc. Rev.* **2012**, *41*, 1323–1349; d) J. Liu, W. Bu, L. Pan, J. Shi, *Angew. Chem.* **2013**, *125*, 4471–4475; *Angew. Chem. Int. Ed.* **2013**, *52*, 4375–4379; e) L. Cheng, C. Wang, Z. Liu, *Nanoscale* **2013**, *5*, 23–37; f) H. H. Gorris, O. S. Wolfbeis, *Angew. Chem.* **2013**, *125*, 3668–3686; *Angew. Chem. Int. Ed.* **2013**, *52*, 3584–3600; g) L. T. Su, S. K. Karuturi, J. Luo, L. Liu, X. Liu, J. Guo, T. C. Sum, R. Deng, H. J. Fan, X. Liu, A. I. Y. Tok, *Adv. Mater.* **2013**, *25*, 1603–1607; h) F. Wang, X. Liu, *Acc. Chem. Res.* **2014**,

47, 1378–1385; i) F. Wang, R. Deng, X. Liu, *Nat. Protoc.* **2014**, *9*, 1634–1644.

[2] a) F. Wang, D. Banerjee, Y. Liu, X. Chen, X. Liu, *Analyst* **2010**, *135*, 1839–1854; b) F. Wang, X. Liu, *Chem. Soc. Rev.* **2009**, *38*, 976–989; c) M. Haase, H. Schäfer, *Angew. Chem.* **2011**, *123*, 5928–5950; *Angew. Chem. Int. Ed.* **2011**, *50*, 5808–5829; d) X. Li, F. Zhang, D. Zhao, *Nano Today* **2013**, *8*, 643–676; e) F. C. J. M. van Veggel, C. Dong, N. J. J. Johnson, J. Pichaandi, *Nanoscale* **2012**, *4*, 7309–7321; f) Y. Zhang, L. Zhang, R. Deng, J. Tian, Y. Zong, D. Jin, X. Liu, *J. Am. Chem. Soc.* **2014**, *136*, 4893–4896.

[3] a) M. Yu, F. Li, Z. Chen, H. Hu, C. Zhan, H. Yang, C. Huang, *Anal. Chem.* **2009**, *81*, 930–935; b) D. Tu, L. Liu, Q. Ju, Y. Liu, H. Zhu, R. Li, X. Chen, *Angew. Chem.* **2011**, *123*, 6430–6434; *Angew. Chem. Int. Ed.* **2011**, *50*, 6306–6310; c) W. Zheng, S. Zhou, Z. Chen, P. Hu, Y. Liu, D. Tu, H. Zhu, R. Li, M. Huang, X. Chen, *Angew. Chem.* **2013**, *125*, 6803–6808; *Angew. Chem. Int. Ed.* **2013**, *52*, 6671–6676.

[4] a) Y. Lu, J. Zhao, R. Zhang, Y. Liu, D. Liu, E. M. Goldys, X. Yang, P. Xi, A. Sunna, J. Lu, Y. Shi, R. C. Leif, Y. Huo, J. Shen, J. A. Piper, J. P. Robinson, D. Jin, *Nat. Photonics* **2014**, *8*, 32–36; b) R. Deng, X. Liu, *Nat. Photonics* **2014**, *8*, 10–12.

[5] a) X. Huang, S. Han, W. Huang, X. Liu, *Chem. Soc. Rev.* **2013**, *42*, 173–201; b) H. Q. Wang, M. Batentschuk, A. Osvet, L. Pinna, C. J. Brabec, *Adv. Mater.* **2011**, *23*, 2675–2680.

[6] G. Liu, B. Jacquier, *Spectroscopic Properties of Rare Earths in Optical Materials, Springer Series in Materials Science*, Springer, Berlin/Heidelberg, New York, **2005**.

[7] Q. Dou, Y. Zhang, *Langmuir* **2011**, *27*, 13236–13241.

[8] a) G. Chen, H. Liu, H. Liang, G. Somesfalean, Z. Zhang, *J. Phys. Chem. C* **2008**, *112*, 12030–12036; b) G. Y. Chen, H. C. Liu, H. J. Liang, G. Somesfalean, Z. G. Zhang, *Solid State Commun.* **2008**, *148*, 96–100.

[9] B. Cao, Z. Feng, Y. He, H. Li, B. Dong, *J. Sol-Gel Sci. Technol.* **2010**, *54*, 101–104.

[10] Q. Sun, X. Chen, Z. Liu, F. Wang, Z. Jiang, C. Wang, *J. Alloys Compd.* **2011**, *509*, 5336–5340.

[11] L. Liu, Y. Wang, X. Zhang, K. Yang, Y. Bai, C. Huang, W. Han, C. Li, Y. Song, *Opt. Mater.* **2011**, *33*, 1234–1238.

[12] Y. Bai, Y. Wang, K. Yang, X. Zhang, G. Peng, Y. Song, Z. Pan, C. H. Wang, *J. Phys. Chem. C* **2008**, *112*, 12259–12263.

[13] X. Luo, W. Cao, *J. Mater. Res.* **2008**, *23*, 2078–2083.

[14] O. Lopez, J. McKittrick, L. Shea, *J. Lumin.* **1997**, *71*, 1–11.

[15] J. H. Chung, S. Y. Lee, K. B. Shim, S.-Y. Kweon, S.-C. Ur, J. H. Ryu, *Appl. Phys. A* **2012**, *108*, 369–373.

[16] V. Mahalingam, R. Naccache, F. Vetrone, J. A. Capobianco, *Opt. Express* **2012**, *20*, 111–119.

[17] H.-Q. Wang, T. Nann, *ACS Nano* **2009**, *3*, 3804–3808.

[18] C. Zhao, X. Kong, X. Liu, L. Tu, F. Wu, Y. Zhang, K. Liu, Q. Zeng, H. Zhang, *Nanoscale* **2013**, *5*, 8084–8089.

[19] a) Q. Cheng, J. Sui, W. Cai, *Nanoscale* **2012**, *4*, 779–784; b) W. Yin, L. Zhao, L. Zhou, Z. Gu, X. Liu, G. Tian, S. Jin, L. Yan, W. Ren, G. Xing, *Chem. Eur. J.* **2012**, *18*, 9239–9245.

[20] a) H. Liang, Y. Zheng, G. Chen, L. Wu, Z. Zhang, W. Cao, *J. Alloys Compd.* **2011**, *509*, 409–413; b) L. Jiang, S. Xiao, X. Yang, J. Ding, K. Dong, *Appl. Phys. B* **2012**, *107*, 477–481; c) N. Niu, F. He, S. Gai, C. Li, X. Zhang, S. Huang, P. Yang, *J. Mater. Chem.* **2012**, *22*, 21613–21623; d) P. Ramasamy, P. Chandra, S. W. Rhee, J. Kim, *Nanoscale* **2013**, *5*, 8711–8717; e) Q. Huang, J. Yu, E. Ma, K. Lin, *J. Phys. Chem. C* **2010**, *114*, 4719–4724.

[21] J. Hao, Y. Zhang, X. Wei, *Angew. Chem.* **2011**, *123*, 7008–7012; *Angew. Chem. Int. Ed.* **2011**, *50*, 6876–6880.

[22] a) B. Dong, B. Cao, Y. He, Z. Liu, Z. Li, Z. Feng, *Adv. Mater.* **2012**, *24*, 1987–1993; b) B. S. Cao, Y. Y. He, Z. Q. Feng, Y. S. Li, B. Dong, *Sens. Actuators B* **2011**, *159*, 8–11.

[23] Z. Li, B. Dong, Y. He, Z. Feng, *J. Lumin.* **2012**, *132*, 1646–1648.

[24] a) J. Zhao, D. Jin, E. P. Schartner, Y. Lu, Y. Liu, A. V. Zvyagin, L. Zhang, J. M. Dawes, P. Xi, J. A. Piper, E. M. Goldys, T. M. Monro, *Nat. Nanotechnol.* **2013**, *8*, 729–734; b) Y. Zhang, X. Liu, *Nat. Nanotechnol.* **2013**, *8*, 702–703.

[25] B. Zhou, H. Lin, E. Y.-B. Pun, *Opt. Express* **2010**, *18*, 18805–18810.

[26] X. Zhai, S. Liu, Y. Zhang, G. Qin, W. Qin, *J. Mater. Chem. C* **2014**, *2*, 2037–2044.

[27] a) J. H. Zeng, T. Xie, Z. H. Li, Y. Li, *Cryst. Growth Des.* **2007**, *7*, 2774–2777; b) M.-Y. Xie, X.-N. Peng, X.-F. Fu, J.-J. Zhang, G.-L. Li, X.-F. Yu, *Scr. Mater.* **2009**, *60*, 190–193.

[28] J. Wang, F. Wang, C. Wang, Z. Liu, X. Liu, *Angew. Chem.* **2011**, *123*, 10553–10556; *Angew. Chem. Int. Ed.* **2011**, *50*, 10369–10372.

[29] Y. Zhang, J. D. Lin, V. Vijayaragavan, K. K. Bhakoo, T. T. Y. Tan, *Chem. Commun.* **2012**, *48*, 10322–10324.

[30] G. Tian, Z. Gu, L. Zhou, W. Yin, X. Liu, L. Yan, S. Jin, W. Ren, G. Xing, S. Li, Y. Zhao, *Adv. Mater.* **2012**, *24*, 1226–1231.

[31] a) F. Wang, X. Fan, M. Wang, Y. Zhang, *Nanotechnology* **2007**, *18*, 025701; b) G. Blasse, B. Grabmaier, *Luminescent Materials*, Springer, Berlin/Heidelberg, **1994**.

[32] F. Wang, R. Deng, J. Wang, Q. Wang, Y. Han, H. Zhu, X. Chen, X. Liu, *Nat. Mater.* **2011**, *10*, 968–973.

[33] Q. Su, S. Han, X. Xie, H. Zhu, H. Chen, C.-K. Chen, R.-S. Liu, X. Chen, F. Wang, X. Liu, *J. Am. Chem. Soc.* **2012**, *134*, 20849–20857.

[34] J. Wang, R. Deng, M. A. MacDonald, B. Chen, J. Yuan, F. Wang, D. Chi, T. S. A. Hor, P. Zhang, G. Liu, Y. Han, X. Liu, *Nat. Mater.* **2014**, *13*, 157–162.

[35] J.-C. G. Bünzli, C. Piguet, *Chem. Soc. Rev.* **2005**, *34*, 1048–1077.

[36] Q. Lü, F. Y. Guo, L. Sun, A. H. Li, L. C. Zhao, *J. Appl. Phys.* **2008**, *103*, 123533.

[37] Z. Li, H. Guo, H. Qian, Y. Hu, *Nanotechnology* **2010**, *21*, 315105.

[38] G. S. Yi, G. M. Chow, *Chem. Mater.* **2007**, *19*, 341–343.

[39] a) H. X. Mai, Y. W. Zhang, L. D. Sun, C. H. Yan, *J. Phys. Chem. C* **2007**, *111*, 13721–13729; b) H. Schäfer, P. Ptacek, O. Zerzouf, M. Haase, *Adv. Funct. Mater.* **2008**, *18*, 2913–2918.

[40] F. Wang, J. Wang, X. Liu, *Angew. Chem.* **2010**, *122*, 7618–7622; *Angew. Chem. Int. Ed.* **2010**, *49*, 7456–7460.

[41] Y. F. Wang, L. D. Sun, J. W. Xiao, W. Feng, J. C. Zhou, J. Shen, C. H. Yan, *Chem. Eur. J.* **2012**, *18*, 5558–5564.

[42] G. Chen, J. Shen, T. Y. Ohulchanskyy, N. J. Patel, A. Kutikov, Z. Li, J. Song, R. K. Pandey, H. Ågren, P. N. Prasad, G. Han, *ACS Nano* **2012**, *6*, 8280–8287.

[43] F. Vetrone, R. Naccache, V. Mahalingam, C. G. Morgan, J. A. Capobianco, *Adv. Funct. Mater.* **2009**, *19*, 2924–2929.

[44] a) D. Yang, C. Li, G. Li, M. Shang, X. Kang, J. Lin, *J. Mater. Chem.* **2011**, *21*, 5923–5927; b) B. Zhou, L. Tao, Y. H. Tsang, W. Jin, *J. Mater. Chem. C* **2013**, *1*, 4313–4318.

[45] H. S. Qian, Y. Zhang, *Langmuir* **2008**, *24*, 12123–12125.

[46] X. Liu, X. Kong, Y. Zhang, L. Tu, Y. Wang, Q. Zeng, C. Li, Z. Shi, H. Zhang, *Chem. Commun.* **2011**, *47*, 11957–11959.

[47] Y. Liu, D. Tu, H. Zhu, R. Li, W. Luo, X. Chen, *Adv. Mater.* **2010**, *22*, 3266–3271.

[48] D. Chen, Y. Yu, F. Huang, H. Lin, P. Huang, A. Yang, Z. Wang, Y. Wang, *J. Mater. Chem.* **2012**, *22*, 2632–2640.

[49] a) K. Aslan, C. D. Geddes, *Metal-Enhanced Fluorescence*, Wiley, Hoboken, **2010**, pp. 1–23; b) E. C. L. Ru, J. Grand, N. Félidj, J. Aubard, G. Lévi, A. Hohenau, J. R. Krenn, E. Blackie, P. G. Etchegoin, *Metal-Enhanced Fluorescence*, Wiley, Hoboken, **2010**, pp. 25–65; c) D. J. Ross, N. P. W. Pieczonka, R. F. Aroca, *Metal-Enhanced Fluorescence*, Wiley, Hoboken, **2010**, pp. 67–90; d) K. Munechika, Y. Chen, J. M. Smith, D. S. Ginger, *Metal-Enhanced Fluorescence*, Wiley, Hoboken, **2010**, pp. 91–118.

[50] W. Deng, F. Xie, H. T. M. C. M. Baltar, E. M. Goldys, *Phys. Chem. Chem. Phys.* **2013**, *15*, 15695–15708.

[51] K. Aslan, I. Gryczynski, J. Malicka, E. Matveeva, J. R. Lakowicz, C. D. Geddes, *Curr. Opin. Biotechnol.* **2005**, *16*, 55–62.

[52] a) L. R. P. Kassab, C. B. de Araújo, R. A. Kobayashi, R. d. A. Pinto, D. M. da Silva, *J. Appl. Phys.* **2007**, *102*, 103515; b) L. R. P. Kassab, F. A. Bomfim, J. R. Martinelli, N. U. Wetter, J. J. Neto, C. B. de Araujo, *Appl. Phys. B* **2009**, *94*, 239–242; c) E. Verhagen, L. Kuipers, A. Polman, *Nano Lett.* **2007**, *7*, 334–337; d) T. Som, B. Karmakar, *J. Quant. Spectrosc. Radiat. Transfer* **2011**, *112*, 2469–2479.

[53] W. Feng, L. D. Sun, C. H. Yan, *Chem. Commun.* **2009**, 4393–4395.

[54] S. Schietinger, T. Aichele, H. Q. Wang, T. Nann, O. Benson, *Nano Lett.* **2010**, *10*, 134–138.

[55] H. Zhang, D. Xu, Y. Huang, X. Duan, *Chem. Commun.* **2011**, *47*, 979–981.

[56] H. P. Paudel, L. Zhong, K. Bayat, M. F. Baroughi, S. Smith, C. Lin, C. Jiang, M. T. Berry, P. S. May, *J. Phys. Chem. C* **2011**, *115*, 19028–19036.

[57] M. Saboktakin, X. Ye, S. J. Oh, S.-H. Hong, A. T. Fafarman, U. K. Chettiar, N. Engheta, C. B. Murray, C. R. Kagan, *ACS Nano* **2012**, *6*, 8758–8766.

[58] M. Saboktakin, X. Ye, U. K. Chettiar, N. Engheta, C. B. Murray, C. R. Kagan, *ACS Nano* **2013**, *7*, 7186–7192.

[59] W. Zhang, F. Ding, S. Y. Chou, *Adv. Mater.* **2012**, *24*, OP236–OP241.

[60] Q.-C. Sun, H. Mundoor, J. C. Ribot, V. Singh, I. I. Smalyukh, P. Nagpal, *Nano Lett.* **2014**, *14*, 101–106.

[61] F. Zhang, G. B. Braun, Y. Shi, Y. Zhang, X. Sun, N. O. Reich, D. Zhao, G. Stucky, *J. Am. Chem. Soc.* **2010**, *132*, 2850–2851.

[62] W. Ge, X. R. Zhang, M. Liu, Z. W. Lei, R. J. Knize, Y. Lu, *Theranostics* **2013**, *3*, 282–288.

[63] C. Zhang, J. Y. Lee, *J. Phys. Chem. C* **2013**, *117*, 15253–15259.

[64] H. Zhang, Y. Li, I. A. Ivanov, Y. Qu, Y. Huang, X. Duan, *Angew. Chem.* **2010**, *122*, 2927–2930; *Angew. Chem. Int. Ed.* **2010**, *49*, 2865–2868.

[65] a) Z. Li, S. Chen, J. Li, Q. Liu, Z. Sun, Z. Wang, S. Huang, *J. Appl. Phys.* **2012**, *111*, 014310–014317; b) Z. Q. Li, X. D. Li, Q. Q. Liu, X. H. Chen, Z. Sun, C. Liu, X. J. Ye, S. M. Huang, *Nanotechnology* **2012**, *23*, 025402.

[66] P. Yuan, Y. H. Lee, M. K. Gnanasammandhan, Z. Guan, Y. Zhang, Q.-H. Xu, *Nanoscale* **2012**, *4*, 5132–5137.

[67] N. Liu, W. Qin, G. Qin, T. Jiang, D. Zhao, *Chem. Commun.* **2011**, *47*, 7671–7673.

[68] P. Kannan, F. A. Rahim, R. Chen, X. Teng, L. Huang, H. Sun, D.-H. Kim, *ACS Appl. Mater. Interfaces* **2013**, *5*, 3508–3513.

[69] W. Deng, L. Sudheendra, J. Zhao, J. Fu, D. Jin, I. M. Kennedy, E. M. Goldys, *Nanotechnology* **2011**, *22*, 325604.

[70] L. Sudheendra, V. Ortalan, S. Dey, N. D. Browning, I. M. Kennedy, *Chem. Mater.* **2011**, *23*, 2987–2993.

[71] A. Priyam, N. M. Idris, Y. Zhang, *J. Mater. Chem.* **2012**, *22*, 960–965.

[72] P. Kannan, F. A. Rahim, X. Teng, R. Chen, H. Sun, L. Huang, D.-H. Kim, *RSC Adv.* **2013**, *3*, 7718–7721.

[73] Y.-F. Wang, G.-Y. Liu, L.-D. Sun, J.-W. Xiao, J.-C. Zhou, C.-H. Yan, *ACS Nano* **2013**, *7*, 7200–7206.

[74] T. Kushida, H. Marcos, J. Geusic, *Phys. Rev.* **1968**, *167*, 289–291.

[75] N. Daldosso, D. Navarro-Urrios, M. Melchiorri, L. Pavesi, F. Gourbilleau, M. Carrada, R. Rizk, C. Garcia, P. Pellegrino, B. Garrido, L. Cognolato, *Appl. Phys. Lett.* **2005**, *86*, 261103.

[76] a) P. Cresswell, D. Robbins, A. Thomson, *J. Lumin.* **1978**, *17*, 311–324; b) J. Suyver, A. Aebischer, D. Biner, P. Gerner, J. Grimm, S. Heer, K. Krämer, C. Reinhard, H. Güdel, *Opt. Mater.* **2005**, *27*, 1111–1130; c) C. Reinhard, K. Krämer, D. A. Biner, H. U. Güdel, *J. Chem. Phys.* **2004**, *120*, 3374–3380.

[77] D. Chen, L. Lei, A. Yang, Z. Wang, Y. Wang, *Chem. Commun.* **2012**, *48*, 5898–5900.

[78] Q. Zhan, J. Qian, H. Liang, G. Somesfalean, D. Wang, S. He, Z. Zhang, S. Andersson-Engels, *ACS Nano* **2011**, *5*, 3744–3757.

[79] J. Shen, G. Chen, A.-M. Vu, W. Fan, O. S. Bilsel, C.-C. Chang, G. Han, *Adv. Opt. Mater.* **2013**, *1*, 644–650.

[80] R. Balda, J. I. Peña, M. A. Arriandiaga, J. Fernández, *Opt. Express* **2010**, *18*, 13842–13850.

[81] X. Xie, N. Gao, R. Deng, Q. Sun, Q.-H. Xu, X. Liu, *J. Am. Chem. Soc.* **2013**, *135*, 12608–12611.

[82] a) H. Wen, H. Zhu, X. Chen, T. F. Hung, B. Wang, G. Zhu, S. F. Yu, F. Wang, *Angew. Chem.* **2013**, *125*, 13661–13665; *Angew. Chem. Int. Ed.* **2013**, *52*, 13419–13423; b) Y. Zhong, G. Tian, Z. Gu, Y. Yang, L. Gu, Y. Zhao, Y. Ma, J. Yao, *Adv. Mater.* **2014**, *26*, 2831–2837; c) X. Li, R. Wang, F. Zhang, L. Zhou, D. Shen, C. Yao, D. Zhao, *Sci. Rep.* **2013**, *3*, 3536.

[83] a) W. Zou, C. Visser, J. A. Maduro, M. S. Pshenichnikov, J. C. Hummelen, *Nat. Photonics* **2012**, *6*, 560–564; b) X. Xie, X. Liu, *Nat. Mater.* **2012**, *11*, 842–843.

[84] Z. Yin, Y. Zhu, W. Xu, J. Wang, S. Xu, B. Dong, L. Xu, S. Zhang, H. Song, *Chem. Commun.* **2013**, *49*, 3781–3783.

[85] J. Liao, Z. Yang, H. Wu, D. Yan, J. Qiu, Z. Song, Y. Yang, D. Zhou, Z. Yin, *J. Mater. Chem. C* **2013**, *1*, 6541–6546.

[86] W. Niu, L. T. Su, R. Chen, H. Chen, Y. Wang, A. Palaniappan, H. Sun, A. I. Y. Tok, *Nanoscale* **2014**, *6*, 817–824.

[87] D. J. Gargas, E. M. Chan, A. D. Ostrowski, S. Aloni, M. V. P. Altoe, E. S. Barnard, B. Sanii, J. J. Urban, D. J. Milliron, B. E. Cohen, P. J. Schuck, *Nat. Nanotechnol.* **2014**, *9*, 300–305.